Journal of Innovative Optical Health Sciences
Vol. 5, No. 4 (2012) 1250023 (10 pages)

DOI: 10.1142/S179354581250023X

QUANTIFYING NANOPARTICLE TRANSPORT *IN VIVO* USING HYPERSPECTRAL IMAGING WITH A DORSAL SKINFOLD WINDOW CHAMBER

TREVOR D. MCKEE[*,†,¶], JUAN CHEN[*], IAN CORBIN[*,§], GANG ZHENG[*,‡] and RAMA KHOKHA[*,‡]

[*]*Ontario Cancer Institute*
University Health Network, Toronto, Ontario

[†]*STTARR Innovation Center*
University Health Network, Toronto, Canada

[‡]*Department of Medical Biophysics*
University of Toronto, Toronto, Canada

[§]*Advanced Imaging Research Center*
University of Texas Southwestern Medical Center at Dallas
Dallas, USA

[¶]*tdmckee@alum.mit.edu*

Accepted 28 July 2012
Published 26 November 2012

We have developed a noninvasive imaging method to quantify *in vivo* drug delivery pharmacokinetics without the need for blood or tissue collection to determine drug concentration. By combining the techniques of hyperspectral imaging and a dorsal skinfold window chamber, this method enabled the real-time monitoring of vascular transport and tissue deposition of nanoparticles labeled with near-infrared (NIR) dye. Using this imaging method, we quantified the delivery pharmacokinetics of the native high-density lipoprotein (HDL) and epidermal growth factor receptor (EGFR)-targeted HDL nanoparticles and demonstrated these HDLs had long circulation time in blood stream (half-life >12 h). These HDL nanoparticles could efficiently carry cargo DiR-BOA to extravasate from blood vessels, diffuse through extracellular matrix, and penetrate and be retained in the tumor site. The EGFR targeting specificity of EGFR-targeted HDL (EGFR-specific peptide conjugated HDL) was also visualized *in vivo* by competitive inhibition with excess EGFR-specific peptide. In summary, this imaging technology may help point the way toward the development of novel imaging-based pharmacokinetic assays for preclinical drugs and evaluation of drug delivery efficiency, providing a dynamic window into the development and application of novel drug delivery systems.

1. Introduction

Targeted therapies hold great promise for the treatment of primary and metastatic cancer by sparing injury to normal host tissues and cells. Although small molecular therapies are potentially potent agents, they lack specificity for cancer cells.[1]

Targeting of such agents is limiting as conjugation of homing ligands can alter or even abolish the therapeutic index of the agent, and even the agents that can be successfully targeted only provide a single payload (i.e., one chemotherapeutic agent per target recognition). Larger therapeutic agents, such as gene therapy with herpes simplex oncolytic viral particles (150 nm diameter), offer tumor specificity (e.g., replication only in p53 deficient cells) but encounter increasing amounts of diffusive hindrance within tumors compared to particles less than 30 nm in diameter.[2] These large agents are unable to sufficiently penetrate tumor tissue and thus are unable to replicate and spread effectively within solid tumors, even with direct intratumoral injection.[3] Targeted delivery of therapeutics via nanosized delivery systems offers great potential for improving tumor specificity over small molecular chemotherapy due to enhanced permeability and retention in tumors.[4,5] Delivery is also improved in comparison to gene therapeutic particles, due to better tumor accessibility of these smaller-sized particles.[2,6,7] Combined, these properties provide a very useful platform for preclinical drug development. High-density lipoproteins (HDL) are natural nanoparticles of ultra-small size (5−12 nm) stabilized by apolipoproteinA-I (ApoA-1) protein.[8] Functionally, they facilitate the transport of cholesterol from tissue back to liver for catabolism through a process known as reverse cholesterol transport. The specific receptor involved with HDL cholesterol transport is the scavenger receptor class B type I (SR-BI), which can directly transport cholesterol ester across the cell membrane through a nonendocytic pathway.[9] SR-BI is found in tissues with critical roles in cholesterol metabolism, such as liver, adrenal glands, and ovaries, and is also highly expressed in many cancer cells, particularly in cancers of ovary, colon,[10] lung,[11] prostate,[12] and breast.[13] Van Berkel and others have used natural HDL as a nanocarrier for therapeutics.[14] To date, many synthetic HDL nanoparticles have been developed for cancer theranostics[10,15] as these nanoparticles possess many features that are desirable for drug delivery. They are biocompatible and nonimmunogenic and can carry versatile payloads of cancer theranostics by multiple labeling approaches.[16] Their ultra-small size (<30 nm) enables improved diffusive transport through the tumor interstitium, allowing penetration and accumulation to reach therapeutically relevant concentrations. In addition, their built-in natural SR-BI targeting can be advantageous for many cancer therapies.[17−19] The HDL particles can also be rerouted to other receptors of choice by integrating with different targeting ligands such as the folate,[20] EGF protein,[21,22] and RGD peptide,[23] thus expanding their horizon for cancer targeting.

In addition to therapeutic payloads,these HDL particles can also be loaded with fluorescent dyes to allow the distribution of HDL to be tracked by imaging methods. In this study, we utilized the near-infrared (NIR) probe, DiR-BOA (1,1′-dioctadecyl-3,3,3′,3′-tetramethylindotricarbocyanine iodide bisoleate), and quantified the distribution of HDL particles within an optical dorsal skinfold window preparation. For successful application of HDL-based particles for cancer therapy, detailed knowledge of the pharmacokinetics of HDL tumor targeting is required. Conventional pharmacokinetic analysis involves the determination of drug concentration in blood and tissue samples at different times post drug injection, which offers little information about the transport dynamics of the drug by nanoparticles from blood to tumor after systemic administration. Here, we demonstrated the utilization of dorsal skinfold window preparation for real-time *in vivo* tracking of HDL delivery, allowing a spatially resolved pharmacokinetic assessment of HDL particle transport within the tumor and surrounding tissues.

2. Materials and Methods

2.1. *Preparation of NIR-dye loaded HDL*

Reconstituted HDL(DiR-BOA) particles were prepared according to previously reported method.[20] EGFR-specific peptide, YHWYGYTPQNVI, was synthesized on a PS-3 peptide synthesizer (Protein Technologies). The EGFR-specific peptide was then conjugated to HDL(DiR-BOA) by classical amide reaction to make EGF-HDL(DiR-BOA) particle (the molar ratio of peptide to HDL is 20 to 1).

2.2. *Development of imaging method*

Dorsal skinfold window chambers were prepared in SCID mice as described previously[2] and inoculated with either GFP transfected MOS-1 murine osteosarcoma cells (Figs. 1 and 2), or A549 human lung

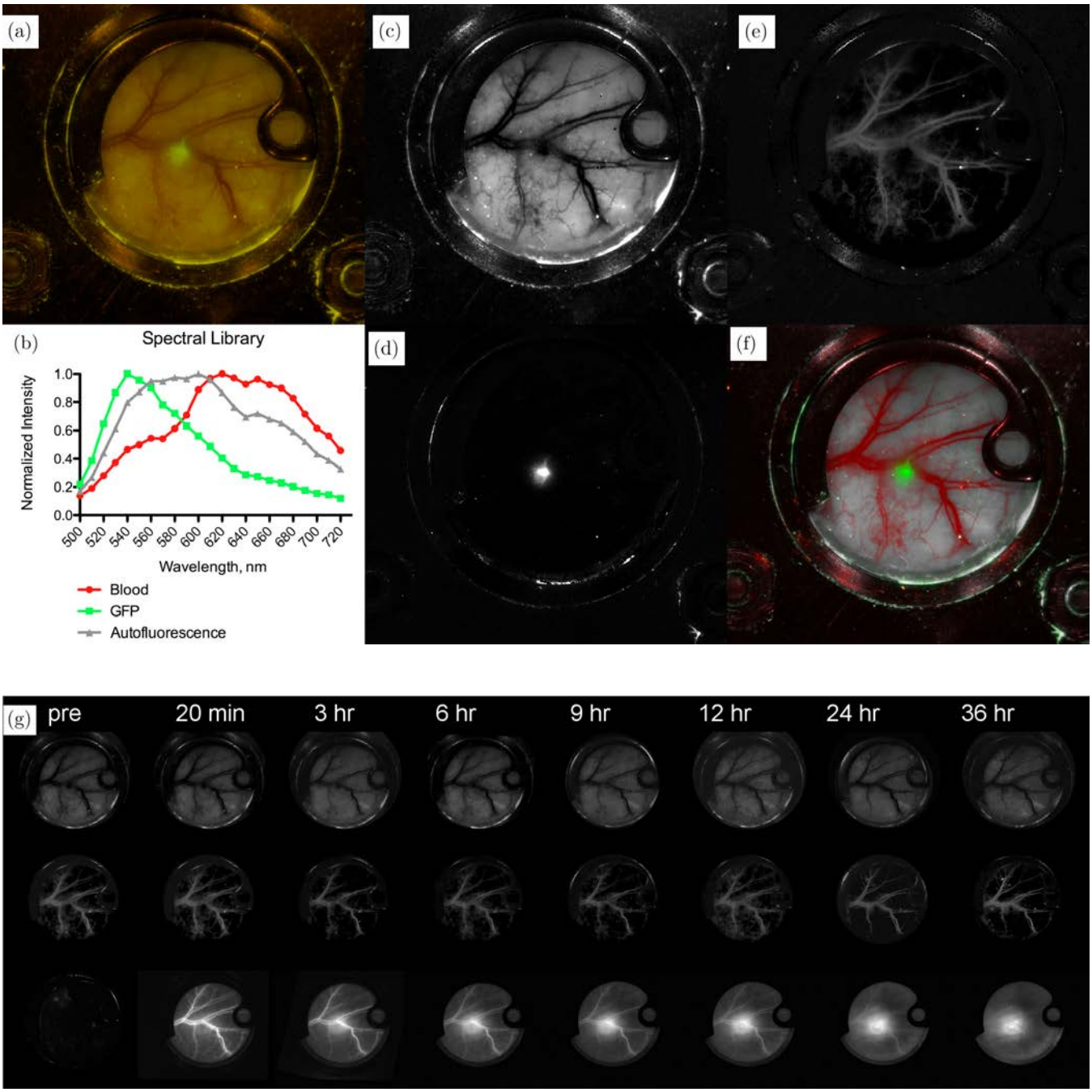

Fig. 1. Nanoparticle distribution within the dorsal skinfold chamber. Mice were injected via tail-vein, and near-infrared (NIR) fluorescence was monitored via the CRI Maestro hyperspectral imaging system. (a) Hyperspectral data cube (10 nm bandwidth channels from 500−720 nm) rendered so as to match the visible spectrum. Spectral components corresponding to GFP, tissue autofluorescence, and hemoglobin were isolated and defined using the spectral library shown in (b), and individual spectrally unmixed channels corresponding to tissue autofluorescence (c), GFP (d), and hemoglobin (e) are shown. (f) An unmixed color composite image is shown, with hemoglobin assigned to the red channel, GFP assigned to the green channel, and tissue autofluorescence assigned to the gray channel. NIR DiR-BOA fluorescence was captured using different excitation and emission filters, with a time course of NIR fluorescence shown in the bottom row of (g) alongside tissue autofluorescence (top row), and hemoglobin (middle row). (h) A color composite of GFP (green), hemoglobin signal (cyan) and HDL (DiR-BOA) nanoparticles (red).

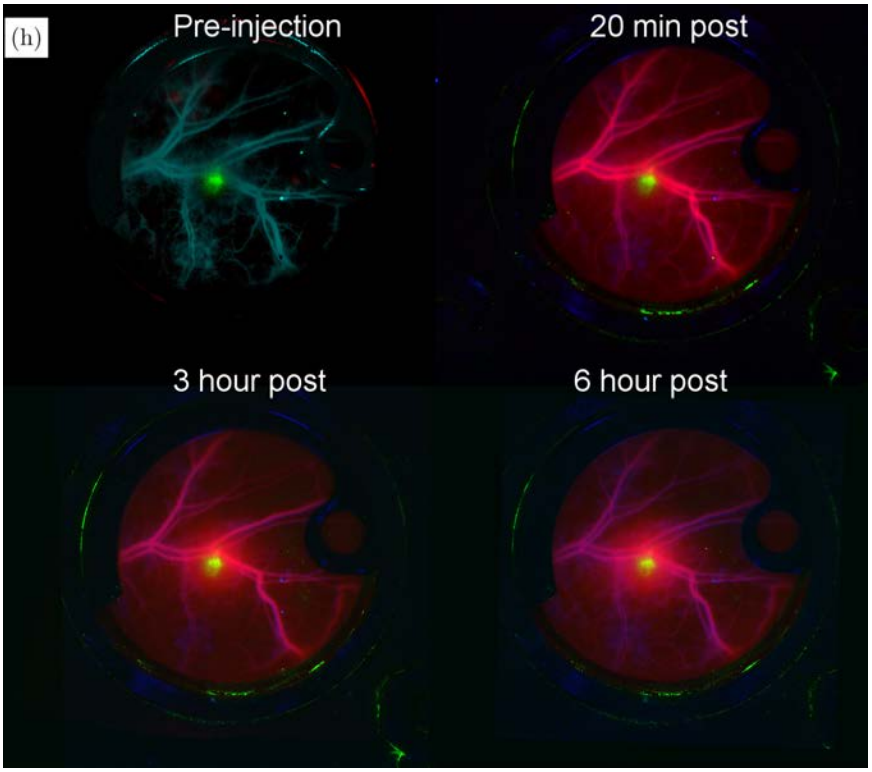

Fig. 1. (*Continued*)

adenocarcinoma cells (Figs. 3 and 4). HDL nanoparticles were then administered via tail-vein injection, and the animals were anesthetized under isofluorane gas and placed in the CRI Maestro hyperspectral imaging system (Caliper Life Sciences, Hopkinton, MA, USA) at the appropriate time points post injection. NIR filter and blue filters were used sequentially to obtain matching NIR and tissue structure maps for co-registration. Following the completion of the imaging time course, the

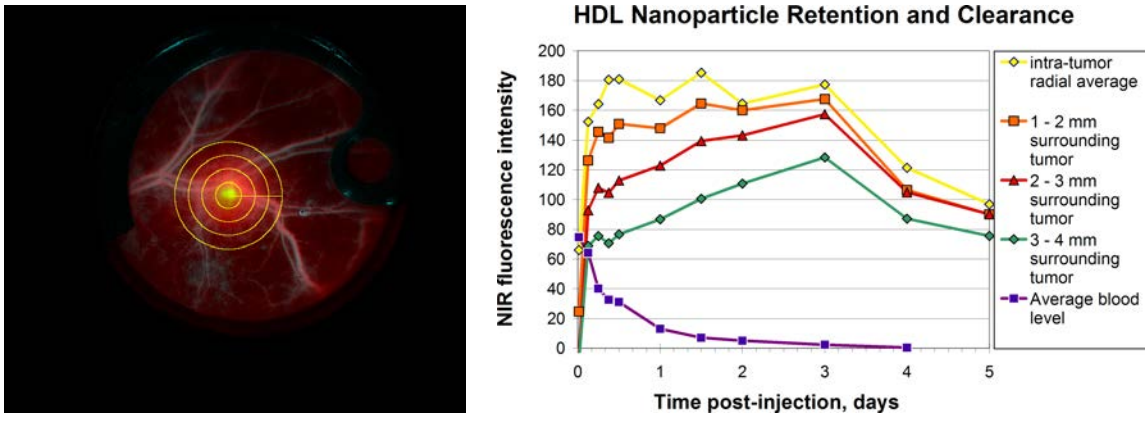

(a) (b)

Fig. 2. Quantitation of nanoparticle distribution within the dorsal skinfold chamber. The isolated NIR spectral component corresponding to nanoparticle distribution within the tumor was analyzed by averaging across a radial profile extending fom the tumor center, with four radial spatial ranges corresponding to 0∼1 mm (within tumor), and tumor periphery: 1∼2 mm, 2∼3 mm, and 3∼4 mm away from the tumor center, as illustrated in (a). The fluorescence intensity within these spatial ranges was quantified in (b). Viewing the data as radial profiles over time, nanoparticle influx occurred gradually up to 36 h post injection (c), with efflux occurring from 36−120 h post injection (d).

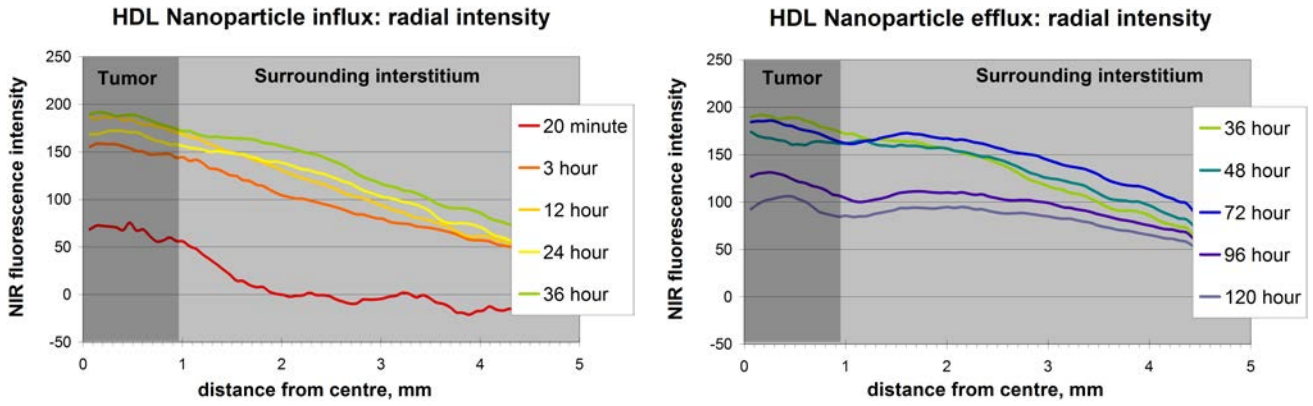

(c) (d)

Fig. 2. (*Continued*)

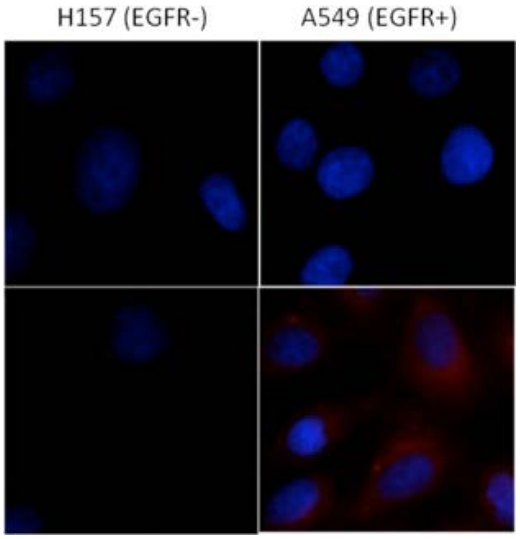

Fig. 3. The fluorescence imaging of the uptake of EGF-HDL (DiR-BOA) on EGFR-positive lung cancer A549 and EGFR-negative lung cancer H157 cells. The results showed the selective uptake of particles in EGFR high-expressed cells.

individual signals for NIR dye (DiR-BOA) (excitation: 710−760 nm; emission: 800 nm long pass), GFP signal from tumor (excitation: 445−490 nm; emission: 515−550 nm), and a signal corresponding to the decreased absorption coefficient of hemoglobin above 600 nm, were extracted using spectral unmixing and either knowledge of pure dye spectra (DiR, GFP), or region of interest (ROI) selection and spectral principal component analysis (blood and tissue autofluorescence). The TurboReg ImageJ plugin,[24] http://bigwww.epfl.ch/thevenaz/turboreg/) was used to obtain registration landmarks in order to align each time point with the previous one, and allow for consistent ROI placement relative to the tumor region. ROIs were selected, and either the average value for that region was calculated over time or a radial profile was calculated using the Radial Profile Plot ImageJ plugin (http://rsbweb.nih.gov/ij/plugins/radial-profile.html), which measures across a radial line centered on the tumor, averaging the image intensity 360° around the central point (placed at the tumor center). The NIR signal intensity values were then graphically plotted over time for tumor and peri-tumor areas, blood vessels, and skin interstitium.

3. Results

3.1. *Developing imaging technique to visualize drug delivery* in vivo

To monitor HDL particles for delivery drugs from blood vessel to tumor site, a NIR dye, DiR-BOA, was loaded in HDL as a drug representative to form HDL (DiR-BOA). Tumor tissue was implanted in a dorsal window chamber using GFP transfected cancer cells (MOS-1 murine transgenic osteosarcoma[25]). Mice were injected with HDL(DiR-BOA) via the tail-vein, and fluorescence was monitored via the CRI Maestro hyperspectral imaging system. The images was acquired using fluorescence imaging across a range of wavelengths, using two excitation/emission filter pairs: NIR filter for DiR-BOA (Ex. 710−760 nm, Em. 800 nm long pass), and Blue filter (Ex. 445−490 nm, Em. 515 nm long pass) for: (i) GFP signal of tumor tissue (Ex. 445−490 nm, Em. 515−550 nm); (ii) tissue autofluorescence

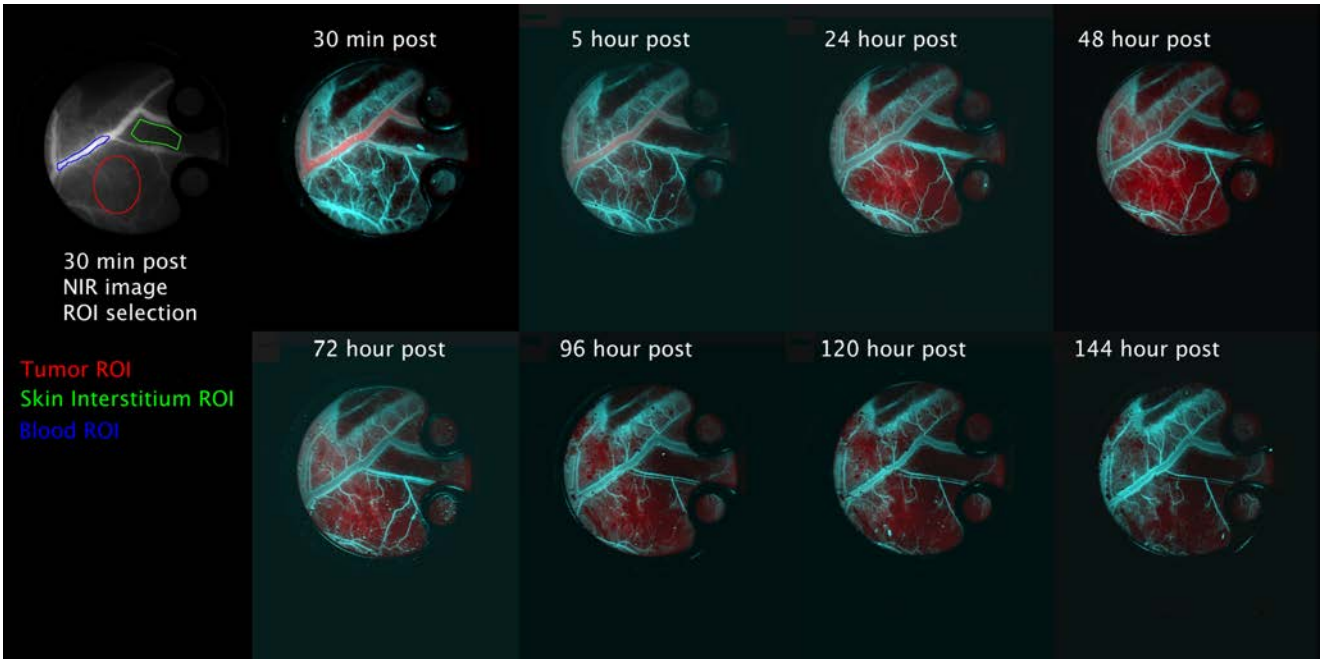

(a)

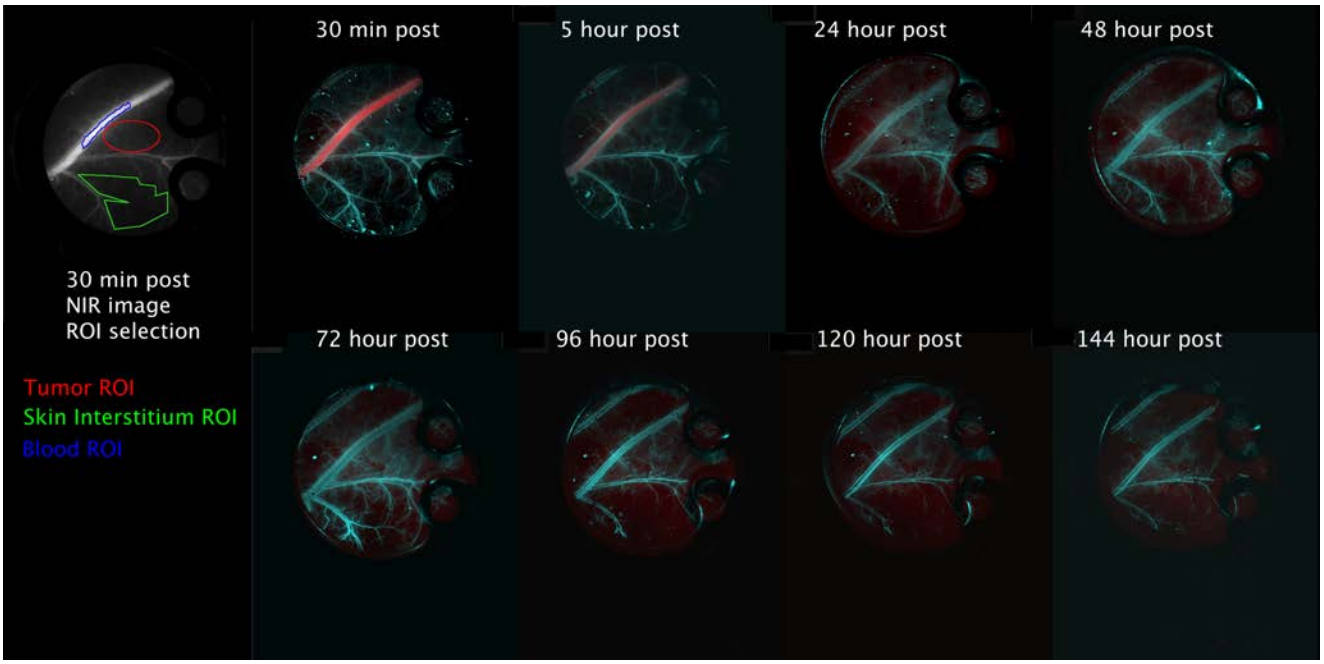

(b)

Fig. 4. Specific targeting of nanoparticles to receptor overexpressed on the surface of tumor cells. Nanoparticles coated with an EGFR-specific peptide were injected into mice either alone (a) or in the presence of competing peptide (b) to demonstrate specificity of uptake. Tumor images were registered to each other, and regions of blood, interstitial skin, and tumor were contoured (as shown) and measured over time in order to determine the kinetics of drug uptake and/or competition. (c) The fluorescence intensity of DiR-BOA in blood, tumor, and interstitium area corresponding to Fig. 4(a). (d) The corresponding fluorescence intensity of DiR-BOA in blood, tumor, and interstitium area for Fig. 4(b).

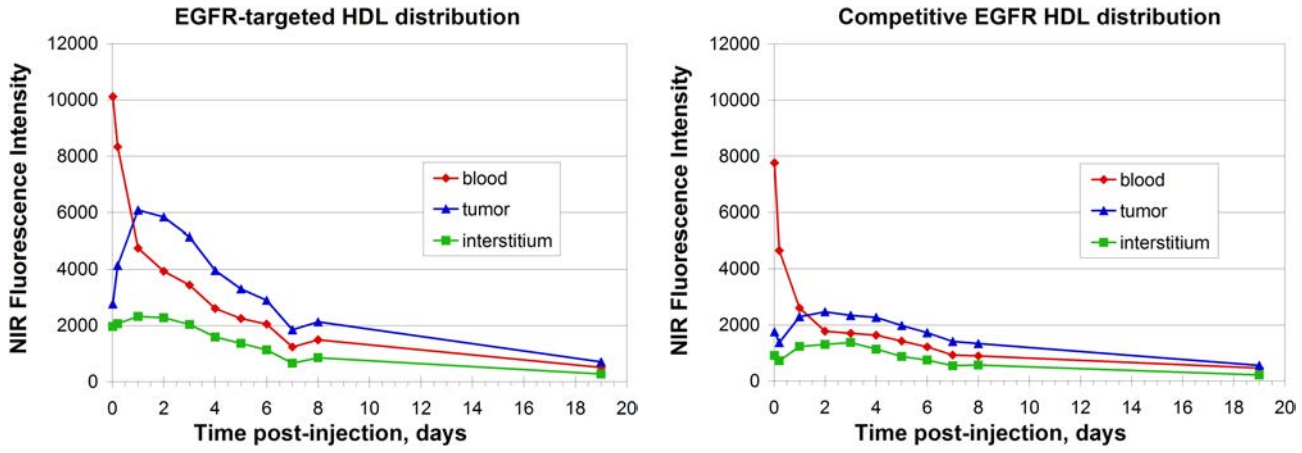

(c) (d)

Fig. 4. (*Continued*)

(Em. 540−600 nm); and (iii) hemoglobin (Em. 600−680). The exact spectra used to unmix the individual components are shown in Fig. 1(b). It should be noted the detection of hemoglobin in this case is likely caused by a shift in tissue autofluorescence in these regions due to the increased molar extinction coefficient of both oxy- and deoxy-hemoglobin below 600 nm, leading to increased absorption of autofluorescence below 600 nm, and a shift in apparent spectral emissions to above 600 nm. Figure 1(a) shows a representation of the hyperspectral image cube from the blue filter, rendered in such a way as to match what would be seen by a camera in the visible spectrum. Spectral libraries were generated from the preinjection timepoint (blue filters), and pure dye (NIR filter), blue filter spectral library shown in Fig. 1 (b), and the hyperspectral image cube was unmixed using these spectra. Figures 1(c), 1(d), and 1(e) show the grayscale individual spectral components corresponding to tissue autofluorescence (c), GFP (d), and hemoglobin (e), with Fig. 1(f) showing a pseudo-colored composite of these signals. As seen in Fig. 1(g), bottom row, there was minimal background fluorescence signal observed in NIR channel (Fig. 1(g), bottom row), indicating that autofluorescence has negligible influence on the quantification of DiR-BOA signal in this study. Images were recorded with matching exposure times and were used to construct a time-dependent fluorescence montage of DiR-BOA using NIR channel (Fig. 1(g), bottom row), showing good blood vessel localization immediately following HDL(DiR-BOA) administration. For comparison, Fig. 1(g) top row shows the tissue autofluorescence, and middle row shows hemoglobin signal, corresponding to each time point NIR image. As time progressed [Fig. 1(g)], the DiR-BOA signal in blood vessels decreased gradually, while the signal in tumor tissue increased over time, peaking at the 24 h time point. After 24 h, the DiR BOA signal in blood vessels was weak while the signal in tumor and peri-tumor rim remained elevated up to 36 h following injection. These data suggested that HDL can deliver cargo via the EPR effect, extravasating from blood vessels, and being selectively retained in the tumor.The spectrally unmixed components corresponding to GFP, tissue hemoglobin autofluorescence, and NIR nanoparticle were re-combined in a pseudo-colored composite [Fig. 1(h)], showing good co-registration between the two image filter sets, with clear visualization of the dynamics of HDL nanoparticle transport.

3.2. *Quantifying the delivery pharmacokinetic of HDL nanoparticle*

We next quantified the fluorescence signal intensity of DiR-BOA in blood and tumor surrounding areas at different times post-injection to determine the pharmacokinetics in detail. This quantification was accomplished with the use of a registration software (TurboReg, Image J), that used manual or automated image registration landmarks to align multiple images together. This software has previously been used to register images obtained from a dorsal skinfold window chamber with sub-cellular accuracy over multiple days, illustrating its potential

utility in this situation.[26] As shown in Fig. 2(a), we quantified the fluorescence of DIR-BOA in four radial spatial ranges, which are 0∼1 mm, 1∼2 mm, 2∼3 mm, and 3∼4 mm distances radially from the tumor center. The time-dependent change in DiR-BOA fluorescence following nanoparticles administration is presented in Fig. 2(b), measured in these radial spatial ranges. The data clearly showed that HDL(DiR-BOA) has long circulation in blood stream, with a half-life time greater than 12 h, which is consistent with the previously reported 15 h based on blood clearance assay.[27] The HDL(DiR-BOA) displayed immediate extravasation within the tumor at 20 min post-injection [Fig. 2(c)], with further increase in tumor accumulation and buildup of a gradient of fluorescence extending away from the tumor into the periphery. The HDL (DiR-BOA) signal demonstrates clear retention and uptake in the tumor and tumor periphery, evidenced by the fact that DiR-BOA signal displayed an increasing trend from blood to tumor 6 h after injection (blood <3−4 mm area <2−3 mm area <1−2 mm area). The influx of DiR-BOA by HDL delivery continued till 36 h post injection, and the efflux slowly processed from 36 h to 120 h [Figs. 2(c) and 2(d)], indicating that the cargo delivered by HDL can be retained in tumors for a long time (>5 days). This is a favorable feature for potential theranostic applications of this drug delivery platform.

3.3. *Developing EGFR-targeted HDL nanoparticles*

We have previously validated the rerouting strategy for HDL nanoparticles.[20] Here we synthesized a EGFR-targeted HDL(DiR-BOA) particles by covalently conjugating particle with an EGFR-specific peptide, YHWYGYTPQNVI.[28] *In vitro* fluorescence microscopy imaging (Fig. 3) confirmed that the resulting EGF-HDL particles selectively bind to EGFR-positive tumor cells. Given that EGFR is overexpressed in many tumor cells, this may prove to be an attractive tumor targeting strategy.

3.4. *Quantifying the selective delivery pharmacokinetic of EGF-HDL nanoparticle*

We next investigated whether we could visualize the selective delivery of HDL nanoparticles to a tumor overexpressing EGFR (A549) using our developed imaging technique. We injected these nanoparticles either alone or with competing free EGFR-specific peptides. As shown in Fig. 4(a), like HDL(DiR-BOA), EGF-HDL(DiR-BOA) demonstrated efficient delivery into the tumor site. As observed by the fluorescence intensity shown in Fig. 4(c), 24 h post-injection, the DiR-BOA signal in tumor was three-fold higher than that in the surrounding skin. Following co-injection of free EGFR-specific peptide [Fig. 4(b)], the delivery of EGF-HDL(DiR-BOA) was significantly inhibited within the first 5 h, as a very low DiR-BOA signal was observed in both tumor and skin interstitium. After 24 h, the signals in both the tumor and interstitium were slightly increased but were much less than that in the mouse without peptide inhibition [Fig. 4(d)]. These data suggested that the EGF-HDL(DiR-BOA) was able to selectively delivered cargo to tumor via EGFR and that we could quantify the selectivity of delivery with our imaging approach. The decrease of inhibition efficiency 5 h after injection could be accounted for the rapid clearance of EGFR-specific peptide (1540.7 Mw) from the circulation.

4. Discussion

Our results indicate that NIR imaging of molecular probes in the dorsal skinfold window model can provide a useful method for *in vivo* noninvasive tracking of biodistribution and pharmacokinetics of the drug delivery system. This technique could potentially obviate the need for sequential blood draws to determine drug concentration. The use of spectral unmixing improves the quantitative ability to relate image-derived intensity to concentration, by minimizing contribution from autofluorescence. Likewise, the pseudo-2D nature of the dorsal chamber in combination with the use of an NIR fluorophore, helps to minimize the effect of absorption and scattering on the fluorescence intensity of the resulting image, allowing us to make the reasonable assumption that fluorescence intensity in the regions of interest is directly proportional to the concentration of fluorophore in that region. The advantages of NIR fluorophores can be observed directly in the unmixed grayscale images in Fig. 1(g), as the NIR channel can visualize more vessels with increased sensitivity and decreased noise in

comparison to the hemoglobin channel, which was collected at lower wavelengths, where absorption and scattering would play more pronounced roles.

We have demonstrated a useful proof of concept that this combination of fluorescent imaging, nanoparticles, and imaging processing technologies allows us to quantify the dymanic pharmacokinetics of nanoparticle transport from blood vessels to tumor-specific sites. This technology may provide a powerful novel method for application toward preclinical drug development and pharmacokinetic assessment, aiding in the rapid evaluation of nanoparticles for efficient and selective delivery of therapeutics.

This technique could, in principle, be applied to any NIR molecular probe, and even multiplexed with multiple fluorophores, assuming reasonably separable emission wavelengths. Combining spectral unmixing with this window chamber preparation and novel probe chemistries opens a wider array of possibilities of using multiple NIR molecular probes to simultaneously assay specific biological activities such as metalloproteinase activity (via cleavable probes) or cellular biodistribution (via cell labeling).

In addition, the techniques described here could also have applications in other biological model systems. The mouse ear is a convenient pseudo-two-dimensional tissue that is very accessible to imaging, allowing for noninvasive tracking of nanoparticle clearance kinetics in any mouse model system. This technique may be particularly useful in pharmacokinetic studies with genetically engineered mouse models of human disease.

5. Summary

In this study, GFP transfected tumor was developed in the dorsal skinfold window chamber mouse model; a NIR dye, DiR-BOA, was loaded in HDL as a drug representative; and a CRI Maestro hyperspectral imaging system was used to monitor and quantify the delivery pharmacokinetic of HDL nanoparticles in a time-dependent fashion. HDL particles, either in native-targeted form or conjugated with EGFR-specific peptide, are observed to exhibit long circulation time in blood stream (half-life >12 h), matching with previous by known pharmacokinetic information of these same compounds. HDL particles are shown to carry cargo DiR-BOA, diffuse through the extracellular matrix, and finally penetrate and retain in tumor site. The novel application of this imaging technology to the study of drug transport *in vivo* may help point the way toward the development of optical pharmacokinetic assessments to improve preclinical drug testing and evaluation of drug delivery systems, providing a novel approach to increasing the throughput of the drug discovery and development process.

Acknowledgments

This work was supported by a Department of Defense Breast Cancer Research Program Idea Award, the Susan G. Komen Foundation, Princess Margaret Hospital Foundation, Canadian Institute of Health Research, and Joey and Toby Tanenbaum/Brazilian Ball Chair in Prostate Cancer Research, University Health Network.

References

1. R. Ng, N. Better, M. D. Green, "Anticancer agents and cardiotoxicity," *Semin. Oncol.* **33**(1), 2–14 (2006).
2. A. Pluen *et al.*, "Role of tumor-host interactions in interstitial diffusion of macromolecules: cranial versus subcutaneous tumors," *Proc. Natl. Acad. Sci. USA* **98**(8), 4628–4633 (2001).
3. T. D. McKee *et al.*, "Degradation of fibrillar collagen in a human melanoma xenograft improves the efficacy of an oncolytic herpes simplex virus vector," *Cancer Res.* **66**(5), 2509–2513 (2006).
4. H. Maeda *et al.*, "Tumor vascular permeability and the EPR effect in macromolecular therapeutics: a review," *J. Control Release* **65**(1–2), 271–284 (2000).
5. F. Yuan *et al.*, "Vascular permeability in a human tumor xenograft: molecular size dependence and cutoff size," *Cancer Res.* **55**(17), 3752–3756 (1995).
6. S. K. Hobbs *et al.*, "Regulation of transport pathways in tumor vessels: role of tumor type and microenvironment," *Proc. Natl. Acad. Sci. USA* **95**(8), 4607–4612 (1998).
7. H. Cabral *et al.*, "Accumulation of sub-100 nm polymeric micelles in poorly permeable tumours depends on size," *Nat. Nanotechnol.* **6**(12), 815–823 (2011).
8. R. A. Silva *et al.*, "Structure of apolipoprotein A-I in spherical high density lipoproteins of different sizes," *Proc. Natl. Acad. Sci. USA* **105**(34), 12,176–12,181 (2008).

9. W. V. Rodrigueza *et al.*, "Mechanism of scavenger receptor class B type I-mediated selective uptake of cholesteryl esters from high density lipoprotein to adrenal cells," *J. Biol. Chem.* **274**(29), 20,344−20,350 (1999).
10. M. M. Shahzad *et al.*, "Targeted delivery of small interfering RNA using reconstituted high-density lipoprotein nanoparticles," *Neoplasia* **13**(4), 309−319 (2011).
11. A. Hrzenjak *et al.*, "Inhibition of lung carcinoma cell growth by high density lipoprotein-associated alpha-tocopheryl-succinate," *Cell Mol. Life Sci.* **61**(12), 1520−1531 (2004).
12. L. K. Mooberry *et al.*, "Receptor mediated uptake of paclitaxel from a synthetic high density lipoprotein nanocarrier," *J. Drug Target.* **18**(1), 53−58 (2010).
13. P. J. Pussinen *et al.*, "The human breast carcinoma cell line HBL-100 acquires exogenous cholesterol from high-density lipoprotein via CLA-1 (CD-36 and LIMPII analogous 1)-mediated selective cholesteryl ester uptake," *Biochem. J.* **349**(2), 559−566 (2000).
14. M. K. Bijsterbosch, T. J. Van Berkel, "Lactosylated high density lipoprotein: A potential carrier for the site-specific delivery of drugs to parenchymal liver cells," *Mol. Pharmacol.* **41**(2), 404−411 (1992).
15. Z. Zhang *et al.*, "Biomimetic nanocarrier for direct cytosolic drug delivery," *Angew. Chem. Int. Ed. Engl.* **48**(48), 9171−9175 (2009).
16. K. K. Ng, J. F. Lovell, G. Zheng, "Lipoprotein-inspired nanoparticles for cancer theranostics," *Acc. Chem. Res.* **44**(10), 1105−1113 (2011).
17. M. Yang *et al.*, "Attenuation of nontargeted cell-kill using a high-density lipoprotein-mimicking peptide−phospholipid nanoscaffold," *Nanomedicine* (*Lond*) **6**(4), 631−641 (2011).
18. M. Yang *et al.*, "Efficient cytosolic delivery of siRNA using HDL-mimicking nanoparticles," *Small* **7**(5), 568−573 (2011).
19. Lin Q. *et al.*, "Efficient systemic delivery of siRNA by using HDL-mimicking peptide lipid nanoparticles," *Nanomedicine* (*Lond*) accepted (2012).
20. R. I. Corbin *et al.*, "Enhanced cancer-targeted delivery using engineered high-density lipoprotein-based nanocarriers," *J. Biomed. Nanotechnol.* **3**, 1−10 (2007).
21. Z. Zhang *et al.*, "HDL-mimicking peptide-lipid nanoparticles with improved tumor targeting," *Small* **6**(3), 430−437 (2010).
22. H. Jin *et al.*, "Investigating the specific uptake of EGF-conjugated nanoparticles in lung cancer cells using fluorescence imaging," *Cancer Nano* **1**, 71−78 (2010).
23. W. Chen *et al.*, "RGD peptide functionalized and reconstituted high-density lipoprotein nanoparticles as a versatile and multimodal tumor targeting molecular imaging probe," *FASEB J.* **24**(6), 1689−1699 (2010).
24. P. Thevenaz, U. E. Ruttimann, M. Unser, "A pyramid approach to subpixel registration based on intensity," *IEEE Trans. Image Process* **7**(1), 27−41 (1998).
25. S. D. Molyneux *et al.*, "Prkar1a is an osteosarcoma tumor suppressor that defines a molecular subclass in mice," *J. Clin. Invest.* **120**(9), 3310−3325 (2010).
26. J. Y. Perentes *et al.*, "*In vivo* imaging of extracellular matrix remodeling by tumor-associated fibroblasts," *Nat. Methods* **6**(2), 143−145 (2009).
27. S. Eisenberg, H. G. Windmueller, R. I. Levy, "Metabolic fate of rat and human lipoprotein apoproteins in the rat," *J. Lipid. Res.* **14**(4), 446−458 (1973).
28. Z. Li *et al.*, "Identification and characterization of a novel peptide ligand of epidermal growth factor receptor for targeted delivery of therapeutics," *FASEB J.* **19**(14), 1978−1985 (2005).